ACS OMEGA

Open Access

http://pubs.acs.org/journal/acsodf

Article

Study on the Effect of Polymer-Modified Magnetic Nanoparticles on Viscosity Reduction of Heavy Oil Emulsion

Nana Sun,* Jianbo Hu, Yuli Ma, and Hongmei Dong

Cite This: *ACS Omega* 2024, 9, 5002−5013

Read Online

ACCESS | Metrics & More | Article Recommendations

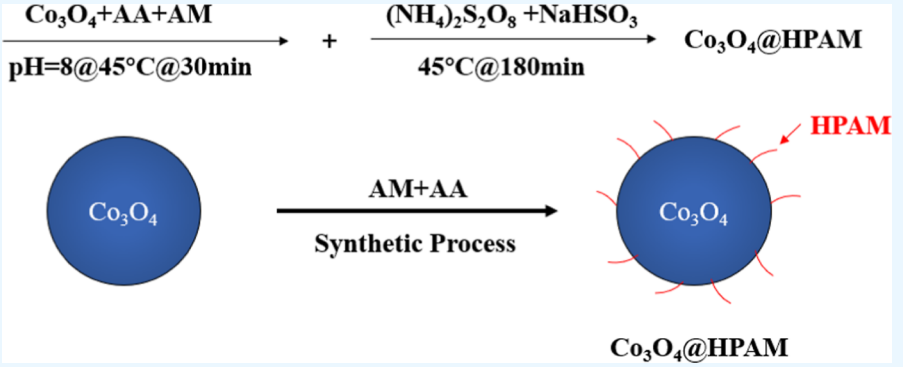

ABSTRACT: To overcome the problems of large dosage, fast sedimentation, and the unsatisfactory emulsification effect of traditional magnetic nanoparticles, polymer-modified magnetic nanoparticle Co_3O_4@HPAM was synthesized as an emulsifier for heavy oil O/W emulsion by modifying the surface of Co_3O_4. The composition of Co_3O_4@HPAM was characterized by Fourier transform infrared spectroscopy, X-ray diffraction analysis, thermogravimetric analysis, and scanning electron microscopy. Then, the effects of the mass fraction of magnetic nanoparticles before and after modification on the stability and rheology of the emulsion were compared and analyzed. The experiments show that the degree of reduction of the water-separation rate under the action of Co_3O_4@HPAM was 13 times higher than that under the action of Co_3O_4 at the same mass fraction. By using Co_3O_4@HPAM, the water separation of the emulsion was only 6.74% at 4 h, while the viscosity reduction was greater than 97% at a mass fraction of 0.04%. Finally, combined with the test results of zeta potential, interfacial tension, contact angle, and oil droplet distribution, the effect mechanism of Co_3O_4@HPAM on the viscosity reduction of heavy oil emulsification was investigated. It is found that the polymer-modified magnetic nanoparticles have stronger negative electricity, a larger contact angle, and smaller interfacial tension, while the oil droplets under their action have a smaller radius and a more homogeneous distribution. The research in this paper provides a theoretical basis for the application of magnetic nanoparticles in heavy oil emulsification and viscosity reduction technology.

1. INTRODUCTION

Heavy oil is rich in asphaltenes, resins, and paraffin, which aggregate together to form a macromolecular structure, resulting in its high viscosity, high density, and poor fluidity, causing problems such as multiphase flow, pipeline clogging, and production interruptions in extraction and transportation.[1,2] Many difficulties in the transportation of heavy and ultraheavy oil limit their economic viability. Therefore, reducing the viscosity and improving the flow of heavy oils become prerequisites for extraction, transportation, and application.

To reduce the difficulty and cost of heavy oil pipeline transportation, scholars at home and abroad have put forward a variety of viscosity reduction and drag reduction techniques, including heating viscosity reduction,[3] microbial viscosity reduction,[4] dilution viscosity reduction,[5] ultrasounds viscosity reduction[6] and reforming viscosity reduction[7] and so on. Each method has its advantages and disadvantages, such as the heating viscosity reduction method, because the heavy oil has good sensitivity to the temperature; the heating method is one of the most commonly used methods for heavy oil gathering and transportation, but this method has high energy consumption and poor economic adaptability to some high viscosity heavy oil. The microbial viscosity reduction method is

Received: November 22, 2023
Revised: December 29, 2023
Accepted: January 5, 2024
Published: January 19, 2024

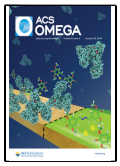

to reduce the viscosity of heavy oil by the microbial degradation of long-chain alkanes in crude oil. However, the microbial viscosity reduction technology also has some limitations, such as the difficulty of culture and screening of strains. The doping thinning viscosity reduction method, according to the principle of "similar miscibility", is to reduce the viscosity of the heavy oil by adding light oil products such as condensate, light crude oil, and naphtha into heavy oil. The effect of viscosity reduction is good, but for the areas with insufficient sparse oil resources, this application is limited. Ultrasound viscosity reduction method uses ultrasounds to modify the heavy oil, irreversibly change the chemical composition of the heavy oil, and then improve the rheological properties of the heavy oil, but ultrasound is harmful to human health and has low economic benefit. Therefore, it is applicable only to a small amount of crude oil extraction. The modified viscosity reduction method is to carry out catalytic cracking of heavy oil to radically reduce the viscosity of heavy oil so that it meets the requirements of pipeline transportation, but the method has the disadvantage of large investment in equipment and high cost.[8]

Another better viscosity reduction method is to emulsify the heavy oil into O/W emulsion. Emulsification technology has the characteristics of a significant viscosity reduction effect, wide selectivity, and high technical and economic value.[9] This method is also a transportation technology that has been tried and studied at home and abroad in recent years. At present, surfactants are mostly used in emulsifying heavy oil, but when surfactants are used as emulsifiers, they have a certain degree of toxicity and some defects such as large dosage, limited scope of application, poisoning of the catalyst, and so on. After emulsification, they will remain in the water or oil phase, which will pollute the environment and cause the problem of emulsion breaking difficulty.[10] Traditional emulsification viscosity reduction technology has insurmountable disadvantages. Therefore, it is urgent to develop a new type of efficient emulsifier.

Fortunately, magnetic nanoparticles (MNPs) have attracted the interest of scholars as a new type of emulsifier that is pollution-free, is easy to recycle, and can be used repeatedly. Józefczak and Wlazło[11] found that solid MNPs were strongly adsorbed at the oil−water interface and were able to stabilize the oil−water interfacial film. Shirokikh et al.[12] found that the aggregation rate of dispersed phase droplets decreases with the increase of MNP concentration, but most of the unmodified MNPs have the disadvantages of high dosage and high cost. Therefore, to achieve the purpose of use, some scholars began to propose functionalized MNPs to modify the surface of MNPs.

By designing the properties of the target products, scholars began to carry out targeted research on modified MNPs: Yue et al.[13] prepared a novel amphiphilic Janus MNP (MJNP) and tested the crystal structure, shape, size, surface composition, and magnetic responsiveness of Janus nanoparticles. The results showed that the high-performance MJNP prepared by the Pickering emulsion method coupled carboxyl and octyl chemical groups at both ends of its surface. These emulsions made from higher concentrations of MJNP have a finer stability and high-temperature resistance. What is more, MJNP has excellent magnetic responsiveness for efficient reusability. Zhang et al.[14] prepared dual-responsive MNPs with Fe_3O_4 and C_{12}min and found that the stability of the emulsion was enhanced under its action. This is due to the combination of negatively charged Fe_3O_4 nanoparticles and positively charged $[C_{12}min]^+$, which changes the three-phase contact angle of the nanoparticle and enhances the hydrophobicity. Luo et al.[15] used the redox-active molecule acetylferrocene azine (Fc^+A) to modify the MNPs Fe_3O_4@SiO_2 with noncovalent hydrophobicity. The modified particles are used as emulsifiers to prepare Pickering emulsion, which has good stability and dual responsiveness, and the stability of the emulsion can be reversibly regulated by redox and magnetic fields. Gálvez-Vergara et al.[16] used polystyrene-modified MNPs (PS-MNPs) to prepare switchable Pickering emulsions in a mixture of polar solvents (e.g., chloroform) and water. The surface of bMNPs was modified by free radical polymerization to make the nanoparticles have stronger hydrophobic properties. Grein-Iankovski et al.[17] modulated the surface properties and interfacial properties of magnetic iron oxide nanoparticles by simply grafting a binary mixture of poly(ethylene oxide) and poly(methyl methacrylate) onto the magnetic iron oxide nanoparticles, which endowed the magnetic iron oxide nanoparticles with surface amphiphilicity. It exhibits stronger adsorption at the toluene/water interface and can stabilize the oil-in-dual-water emulsion. Uhlmann et al.[18] found that the stability of emulsions can be improved by attaching polymers to the surface of nanoparticles, which is due to the modulation of the interfacial properties, surface morphology, wettability, permeability, and adhesive properties of the nanoparticles. Sun et al.[19] studied the preparation of polymer-based modified MNPs. The experiments show that the modified MNPs have different effects on the stability of emulsion under different pH conditions, and the effect is significantly better than that of the unmodified MNPs. Although the research on modified MNPs is increasing at present, it is not difficult to find that the mechanism of modified MNPs to emulsify and reduce the viscosity of heavy oil is still poorly understood, and many scholars have failed to solve the problem of rapid settlement of MNPs by modification of MNPs, resulting in a large number of MNPs, which makes it difficult to realize the dilemma of popularization and application.

Based on the previous studies by scholars and research groups, this paper considers the design of a highly dispersed polymer-based modified MNP to further improve the stability of the emulsion. On this basis, the water-separation rate and viscosity reduction rate are used as the evaluation indexes to analyze the influence law of the mass fraction of MNPs before and after modification on the stability and rheological properties of heavy oil-in-water emulsions. Then, the emulsification and viscosity reduction mechanism of the modified MNPs was elaborated from the microscopic point of view by comparing the electrification and contact angle of MNPs before and after the modification as well as the interfacial tension between oil and water and the distribution of oil droplets. The research in this paper provides the theoretical basis and technical guidance for the application of modified MNPs in heavy oil emulsification and viscosity reduction transportation technology.

2. EXPERIMENTAL SECTION

2.1. Reagents and Instruments. The oil used in the experiment was Karamay heavy oil with water content <0.10%, and the density was 954.15 kg·m^{-3} at 25 °C. The viscosity−temperature curve of the heavy oil is shown in Figure 1. The apparent viscosity of the heavy oil was 25.69 Pa·s when the temperature was 25 °C and the shear rate was 10 s^{-1}.

https://doi.org/10.1021/acsomega.3c09337
ACS Omega 2024, 9, 5002−5013

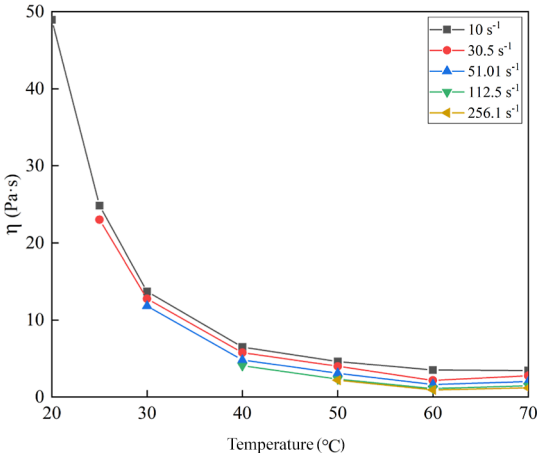

Figure 1. Viscosity-temperature curve of heavy oil

The main experimental drugs were: amphoteric surfactant cocamidopropyl betaine CAB-35 (containing an active ingredient with a mass fraction of 35%), purchased from Shandong Yusuo Chemical Company; Co_3O_4 MNPs, molecular weight: 240.8 g/mol, purchased from Shanghai McLean Biochemical Technology Co; sodium bisulfite $NaHSO_3$, molecular weight: 104.06 g/mol; and ammonium persulfate $(NH_4)_2S_2O_8$, molecular weight: 228.20 g/mol analytically pure, purchased from Tianjin Zhiyuan Chemical Reagent Co. Citric acid, molecular weight: 210.14 g/mol, was purchased from Tianjin Baishi Chemical Co. Gelatin was purchased from Tianjin Guangfu Fine Chemical Research Institute. Acrylamide (AM), molecular weight: 71.08 g/mol, acrylic acid (AA), molecular weight: 207.70 g/mol, acetone, and ethanol were purchased from Shanghai Aladdin Biochemical Co. Petroleum ether and NaOH (analytically pure) were purchased from Hongyan Reagent Factory, Hedong District, Tianjin. The experimental water was distilled water, which was self-made in the laboratory.

Laboratory apparatus: BS-224S Electronic balance, Beijing Sartorius Instrument System Co., Ltd.; JY5002 Electronic balance, Shanghai Shunyu Hengping Scientific Instrument Co, Ltd.; Ultrasounds Cell Crusher, Shanghai Hushan Industrial Co., Ltd.; JJ-1A Digital display Electric Mixer, Changzhou Putian instrument Manufacturing Co., Ltd.; HH-2 Digital display constant temperature Water Bath, Jintan Huafeng Instrument Co., Ltd.; Electrothermal constant temperature water bath, Shanghai Keheng Industrial Development Co., Ltd.; Nano ZS90 zeta potential Analyzer, Malvern, UK; Motic microscope, Xiamen McAudi Optical Instrument Co., Ltd.; JC2000D2 contact Angle Meter, Shanghai Zhongchen Digital Equipment Co. Ltd.; Beaker, measuring cylinder, colorimetric tube, and pipet, Sichuan Shuniu Glass Instrument Co., Ltd.

2.2. Synthetic Experiments. *2.2.1. Synthesis of HPAM.* Equal amounts of AM and AA are weighed, and a certain quantity of distilled water (accounting for 15% of the monomer mass) is added to them. The solution is fully dissolved by stirring with a glass rod; then, the solution is adjusted to pH 8, poured into a three-necked flask, and placed it in a constant temperature water bath set at 45 °C. The stirrer is turned on to adjust the speed to 600 rpm, and after ventilating nitrogen for 30 min, 0.3% (by monomer mass) of ammonium persulfate is added to it, and 0.2% (by mass of monomer) sodium bisulfite solution is added after 5 min. After addition of sodium bisulfite, the gas source was turned off and the rotational speed adjusted to 300 rpm for 3 h to obtain anionic polyacrylamide colloids. It was then removed, dried, immersed in acetone for 24 h, and then soaked in anhydrous ethanol for 24 h to remove homopolymers and residual monomers. The obtained white solid was dried in a constant temperature drying oven and then pulverized to obtain a powder sample of anionic polyacrylamide.

2.2.2. Synthesis of Co_3O_4@HPAM. Using the aqueous method, AM (15%), AA (15%), Co_3O_4 (9%), citric acid (2%), and gelatin (3%) were dissolved in distilled water. The solution was stirred well with a glass rod and after completely dissolving and fully mixing, the solution was poured into a three-necked flask and placed in a thermostatic water bath with the temperature set at 45 °C. After injecting nitrogen into the flask and stirring the solution for 30 min, the initiator dissolved in distilled water was added dropwise to the flask and stirred for 3 h to get a black gel, which was washed with acetone and anhydrous ethanol. Then, the product was dried to a constant weight in a blast furnace at 70 °C, cooled, and pulverized to obtain a powder of polymer-based modified MNPs, which is tested for its properties. The synthesis process is shown in Figure 2, and the experimental setup is schematically shown in Figure 3.

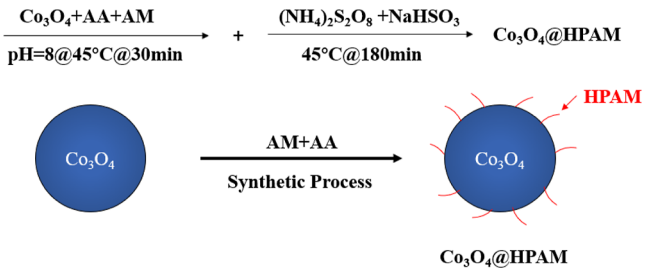

Figure 2. Surface of Co_3O_4 modified by modification

2.3. Dispersion Testing. The MNP solution with the same mass fraction before and after modification was prepared with laboratory-made distilled water, which was placed under an ultrasound cell crusher for 20 min to make it fully dispersed, and then quickly poured into the sampling bottle to observe and record its settlement, as shown in Figure 4 below.

Recording immediately after the end of the sonication, as shown in Figure 4a, it can be noticed that the unmodified MNPs have settled, and the modified MNPs have good dispersibility; at resting for 120 min, as shown in Figure 4b, the unmodified MNPs have precipitated completely, while the modified MNPs still maintain good dispersibility. The experimental results show that the dispersion of the modified MNPs Co_3O_4@HPAM is significantly stronger than that of the unmodified MNPs Co_3O_4.

2.4. Characterization Experiments. Fourier transform infrared (FTIR) spectroscopy (Nicolet iS 50), Thermo Fisher Scientific (China) Co. Ltd., was used to determine the functional groups and chemical bonds in the synthesized Co_3O_4@HPAM; The X-ray diffractometer (XRD-6100), Shimadzu (Shanghai) Laboratory Equipment Co. Ltd., used Cu Kα radiation in the 2θ range from 10 to 80° to obtain the composition and morphology of Co_3O_4@HPAM, HPAM, and Co_3O_4 crystals; The thermogravimetric analyzer (TGA-601), Nanjing Huicheng Instrumentation Co., Ltd., was heated to 800 °C at a heating rate of 10 °C/min in a nitrogen

https://doi.org/10.1021/acsomega.3c09337
ACS Omega 2024, 9, 5002−5013

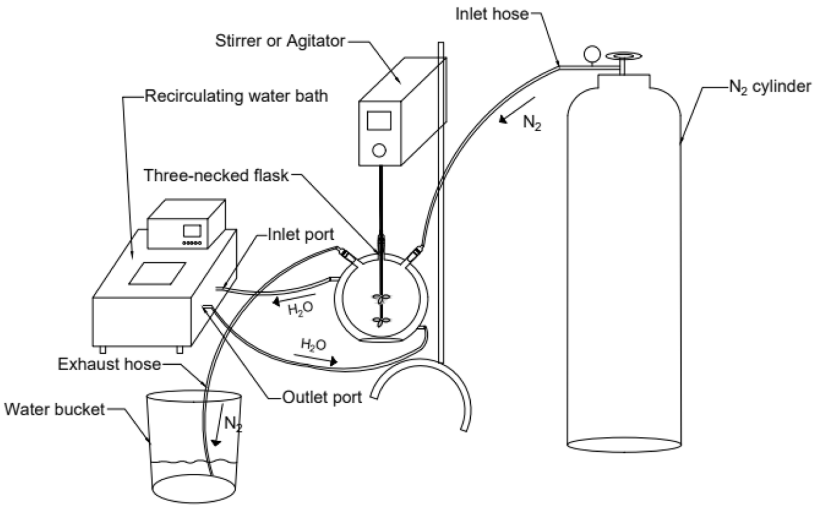

Figure 3. Schematic diagram of the synthesis device

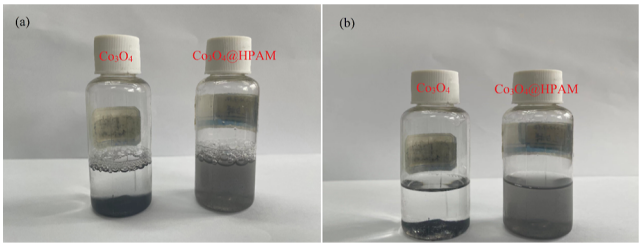

Figure 4. Dispersion of MNPs before and after modification. (a) Dispersion at static 0 min. (b) Dispersion at static 120 min

environment to test the thermal stability of MNPs before and after modification.

2.5. Stability Testing. An aqueous solution of CAB-35 with a mass fraction of 0.5% was prepared, and then, different masses of Co_3O_4 or Co_3O_4@HPAM were added to form different mass fractions of binary active water, which is used as the emulsifier in this experiment. The heavy oil was mixed with active water containing the emulsifier according to the mass ratio of 7:3, and then, it was placed in a constant temperature water bath at 25 °C for 30 min and stirred thoroughly with a digital electric stirrer. The stirring speed of the samples was 1000 rpm, and the stirring time was 3 min.

The water-separation rate of the emulsion under different conditions is determined by the bottle test method. The lower the water-separation rate, the better the stability of the emulsion is. The water-separation rate is calculated, as shown in eq 1.

$$f = \frac{V_1}{V_2} \times 100\% = \frac{H_1}{H_2 \times 30\%} = 100\% \quad (1)$$

where f is the emulsion water-separation rate (%), V_1 is the volume of separated water (mL), V_2 is the total volume of water (mL), H_1 is the separation height of the water (mm), H_2 is the total height of emulsion (mm), and 0.3 is the proportion of active water in the emulsion.

2.6. Rheology Testing. According to the apparent viscosity data, the viscosity reduction rate of heavy oil is analyzed, and the calculation formula is shown in eq 2. The lower the apparent viscosity of the emulsion, the higher the viscosity reduction rate of the heavy oil after emulsification. During the experiment, the shear rate is set to 10−300 s^{-1}, the temperature of the temperature control equipment of the rheometer is adjusted to the experimental temperature, and then the refrigeration and circulation are turned on. When the temperature reaches the experimental temperature, the stirred sample is immediately poured into the rotor and then the rotor is mounted on the rheometer. Under these conditions, the apparent viscosity of the emulsion at different shear rates is measured.

$$n = \frac{\eta_1 - \eta_2}{\eta_1} \times 100\% \quad (2)$$

where n is the viscosity reduction rate (%), μ_1 is the heavy oil viscosity (Pa·s), and μ_2 is the emulsion viscosity (Pa·s).

2.7. Zeta Potential. The binary-activated water containing different mass fractions of MNPs before and after modification was dispersed by ultrasonic treatment for 5 min, and the samples were put into the zeta potential cuvette by using a syringe. Meanwhile, it is checked that there are no bubbles in the cuvette; then, it is put into the zeta potential instrument paying attention to the side with the engraved Malvern lettering facing toward itself, and the lid of the instrument is closed; the zeta potential mode in the test software is selected, the measurement option is clicked to set the sample name, and then the test is started; each sample was measured three times, and the results were averaged.

2.8. Wettability. The MNPs and CAB-35 before and after modification were configured into a certain concentration of mother liquid, and then, it was dispersed by ultrasonic treatment for 40 min. The mother liquid of MNPs was dripped onto the glass slide by a glue head eyedropper, then put into a drying box, and dried at 50 °C to form a uniform and dense film on its surface. The deionized water droplets of 3 μL were taken on the slide with a microsampler, and the contact angle was measured by a contact angle meter. Each sample was measured three times, and the results were averaged.

2.9. Interface Tension. First, start the spin-drop interface measuring instrument, open the measurement software, and preheat the instrument for 10 min; second, use the 1 mL syringe to inject the high-density phase (active water) into a quartz tube with a diameter of 0.5 cm, then use the syringe again to inject the measured oil phase into the activated water of the quartz tube to ensure that there are no small bubbles

https://doi.org/10.1021/acsomega.3c09337
ACS Omega 2024, 9, 5002−5013

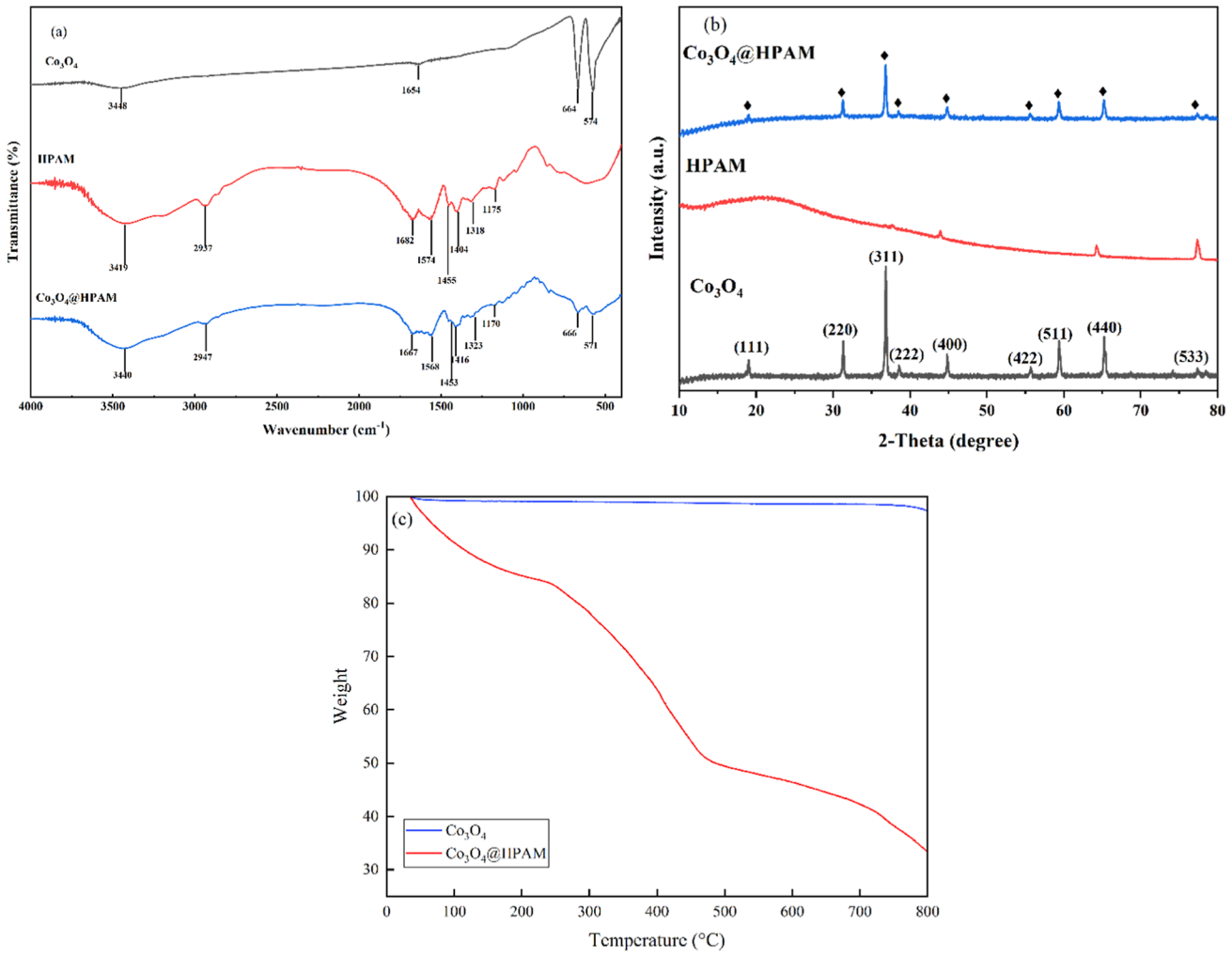

Figure 5. Physical characterization of MNPs before and after modification. (a) FTIR. (b) X-ray powder diffraction. (c) Thermogravimetric analysis (TGA)

inside, and then insert the calibrated needle to carry out the amplification factor of the activated water containing ionic liquids. After the calibration is completed, rinse the quartz tube, reinject the binary active water and oil phase with different mass fractions before and after modification, and then put the quartz tube into the measuring cell of the instrument. After fixing it, the rotational speed was adjusted to 6000 rpm. Under the action of centrifugal force, on starting the instrument, it can be found that the oil droplets in the quartz tube are stretched into an oval shape. Wait for the shape to stop changing, freeze, and save the image, and then click on the measurement button to calculate its interfacial tension; after the measurement is completed, rinse the quartz tube and continue to prepare for the next measurement.

2.10. Microscopic Morphology. The emulsion under the effect of different mass fractions of MNPs before and after modification was prepared. The emulsion was extracted using a disposable needle and dripped onto the glass slide, and the coverslip was covered. Take out the biological microscope, place the microscope on the test bench, rotate the converter, select the 40× objective lens with the light hole, and place the slide containing the sample on the carrier stage. Turn on the computer and start the software, set the image resolution to 4000 × 3000, and observe the dispersed oil droplets in the water phase while capturing photos on the software. Turn off the power of the software, computer, and microscope after the acquisition.

3. RESULTS AND DISCUSSION

3.1. Characterization of MNPs. To verify the success of the modification of MNPs, we characterized the morphology,

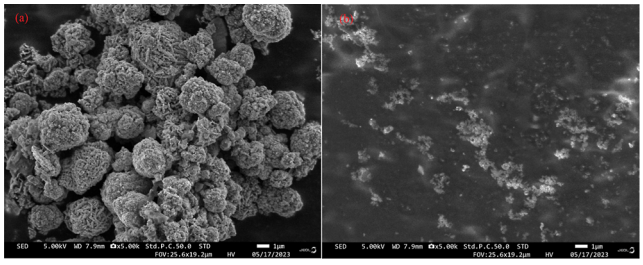

Figure 6. SEM images of Co_3O_4 and Co_3O_4@HPAM: (a) Co_3O_4 (scale is 1 μm); (b) Co_3O_4@HPAM (scale is 1 μm)

structure, and thermal stability of the newly synthesized Co_3O_4@HPAM.

The FTIR spectrum of the Co_3O_4 sample is shown in Figure 5a. There is O−H stretching vibration at 3448 cm^{-1}, H_2O variable angle vibration at 1654 cm^{-1}, and Co_3O_4 infrared

https://doi.org/10.1021/acsomega.3c09337
ACS Omega 2024, 9, 5002−5013

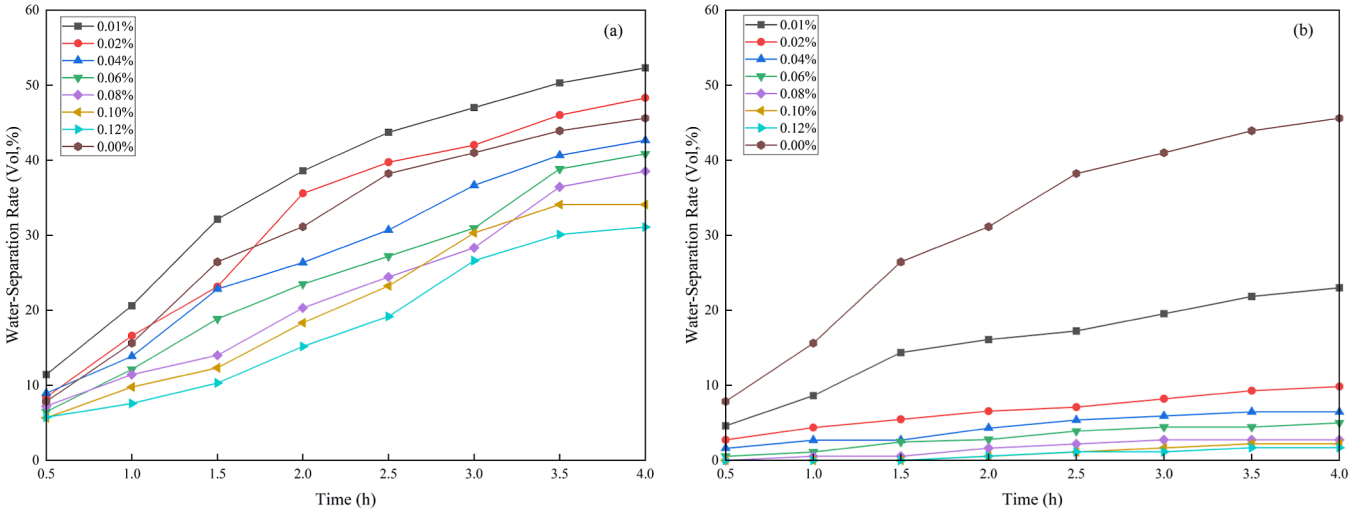

Figure 7. Effect of the Co_3O_4 mass fraction before and after modification on emulsion stability (a) Co_3O_4 (b)Co_3O_4@HPAM

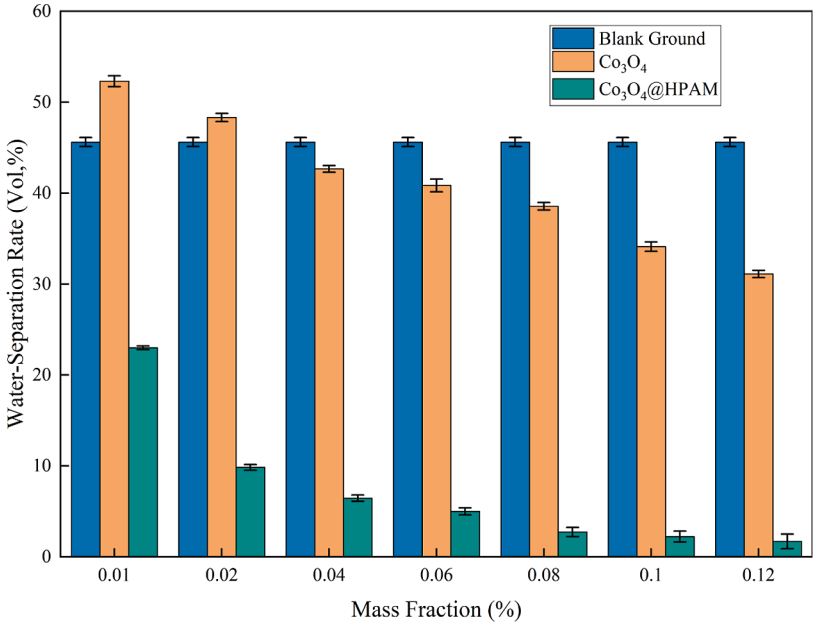

Figure 8. Effect of Co_3O_4 before and after modification on emulsion stability with different mass fractions for 4 h

characteristic peaks at 664 and 574 cm^{-1}.[20] The FTIR spectrum of the HPAM sample is shown in Figure 5a, in which the bending vibration absorption peaks of HPAM are from AM and AA. The characteristic absorption peak of the N−H stretching vibration of the amine group of AM is 3419 cm^{-1}, and the C−H stretching vibration is 2937 cm^{-1}; what is more, the C═O stretching vibration of the amide group of AM is 1682 cm^{-1}; the variable angle vibration of NH_2 is at 1574 cm^{-1}; C−H variable angle vibration is at 1455 cm^{-1}; C−N stretching vibration is at 1404 cm^{-1}; C−O stretching vibration absorption peak in carboxylic acid at 1318 cm^{-1}; and CH_2 out-of-plane rocking vibration is at 1175 cm^{-1}.[21] Through the infrared spectrum analysis of HPAM, it is proved that it conforms to the theoretical structure and is a target anionic polymer.[22] The FTIR spectrum of the Co_3O_4@HPAM sample is shown in Figure 5a. The N−H stretching vibration is at 3440 cm^{-1}; C−H stretching vibration is at 2947 cm^{-1}; C═O stretching vibration is at 1667 cm-1; NH_2 variant angle vibration is at 1568 cm^{-1}; C−H variant angle vibration is at 1453 cm^{-1}; C−N stretching vibration is at 1416 cm^{-1}; CH_2 twisting vibration is at 1323 cm^{-1}; CH_2 out-of-plane rocking vibration is at 1170 cm^{-1}; and Co_3O_4 infrared characteristic peaks are at 666 and 571 cm^{-1}. From the atlas, it is obvious that the sample Co_3O_4@HPAM exhibits the characteristic peaks of both sample HPAM and Co_3O_4. These results prove that Co_3O_4@HPAM has been successfully prepared.

As shown in Figure 5b, the peaks observed in the XRD curves of uncoated Co_3O_4 nanoparticles at $2\theta \approx 18.99$, 31.27, 36.84, 38.54, 44.8, 59.348, and 65.23° correspond to the seven characteristic diffraction peaks, (111), (220), (311), (222), (400), (511) and (440), of Co_3O_4 face-centered cubic crystalline phases with $Fd\bar{3}m$ space group.[23] The HPAM samples mainly contain amorphous phases, which can be observed from the XRD patterns with obvious diffuse bun peaks near 20°. It indicates that the substances mainly exist in amorphous phases, and the 20° position is often found in most amorphous polymers. The characteristic diffraction peaks of Co_3O_4@HPAM are almost the same as those of Co_3O_4, and

https://doi.org/10.1021/acsomega.3c09337
ACS Omega 2024, 9, 5002−5013

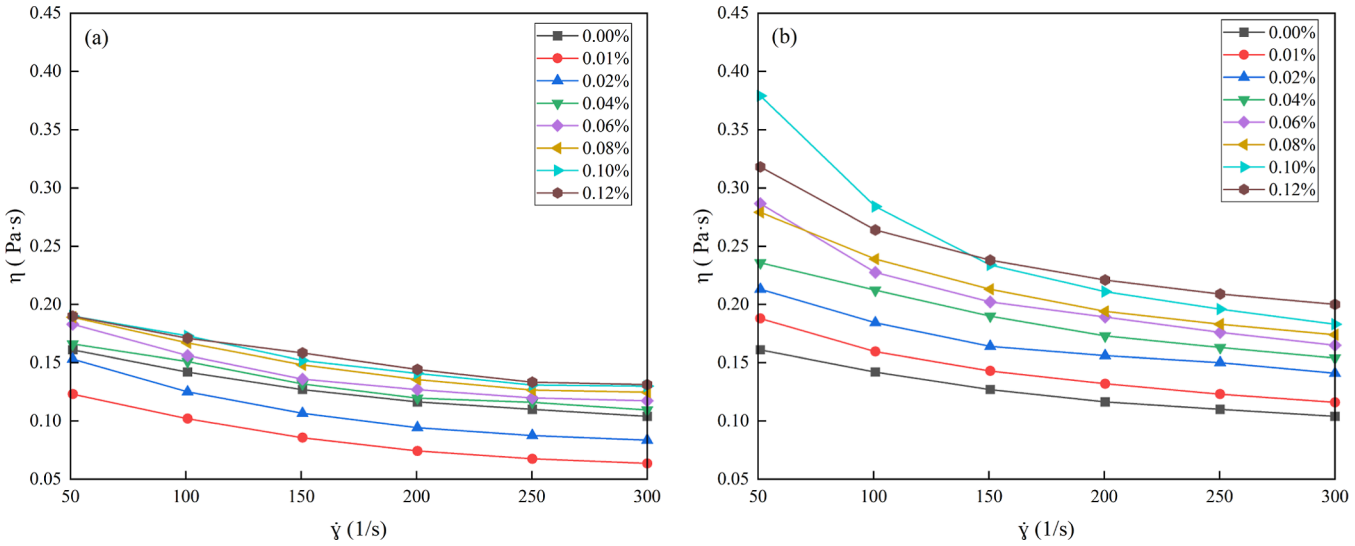

Figure 9. Effect of MNP mass fraction on the apparent viscosity of emulsion before and after modification (a) Co_3O_4 (b) Co_3O_4@HPAM

Table 1. Effect of MNP Mass Fraction on the Viscosity Reduction Rate of Heavy Oil before and after Modification

	n/%							
	γ = 10 s^{-1}		γ = 15.86 s^{-1}		γ = 21.72 s^{-1}		γ = 30.50 s^{-1}	
mass fraction/%	Co_3O_4	Co_3O_4@HPAM	Co_3O_4	Co_3O_4@HPAM	Co_3O_4	Co_3O_4@HPAM	Co_3O_4	Co_3O_4@HPAM
0.01	99.81	99.16	99.88	99.22	99.86	99.2	99.88	99.28
0.02	99.78	98.39	99.81	98.52	99.83	98.66	99.82	98.62
0.04	99.65	98.5	99.67	98.56	99.68	98.53	99.64	98.53
0.06	99.61	97.83	99.63	97.98	99.66	98.07	99.64	98.14
0.08	99.56	97.62	99.59	97.90	99.61	97.86	99.59	98.01
0.10	99.45	97.5	99.52	97.82	99.53	97.58	99.51	97.84
0.12	99.41	97.34	99.45	97.57	99.49	97.23	99.48	97.75

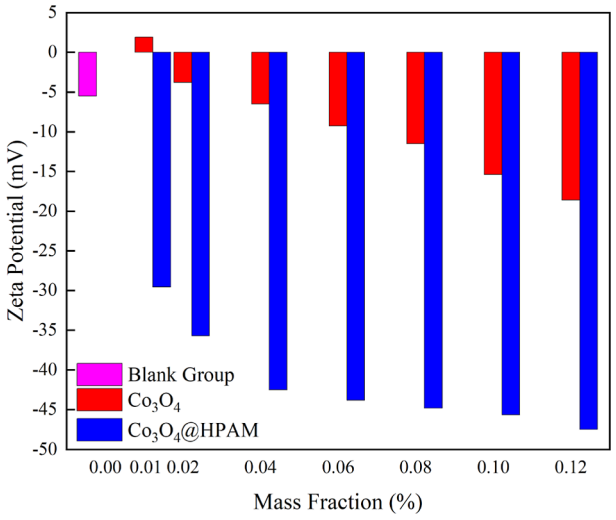

Figure 10. Zeta potential of MNPs with different mass fractions before and after modification.

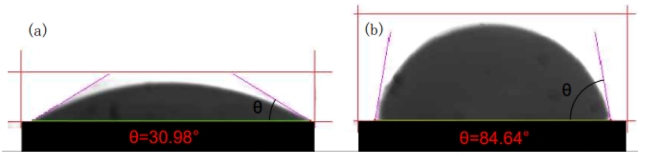

Figure 11. Contact angle of MNPs before and after modification (a) Co_3O_4 (b) Co_3O_4@HPAM

Table 2. Interfacial Tension of MNPs with Different Mass Fractions before and after Modification

mass fraction (%)	Co_3O_4 (mN/m)	Co_3O_4@HPAM (mN/m)
0.00	1.56311	
0.01	1.73212	1.07492
0.02	1.62426	0.85221
0.04	1.48813	0.69382
0.06	1.40114	0.53343
0.08	1.29025	0.48328
0.10	1.21961	0.32541
0.12	1.15453	0.28624

the characteristic diffraction peaks are relatively reduced in intensity and slightly broadened by HPAM, indicating the presence of nonmagnetic and amorphous HPAM coatings on the surface of Co_3O_4, suggesting the successful combination of Co_3O_4 with HPAM.

To study the thermal stability of synthesized Co_3O_4@HPAM, TGA was carried out, and the results are shown in Figure 5c. The thermogravimetric plot of Co_3O_4 shows two inflection points. The first inflection point is 35−180 °C corresponding to a weight loss of 0.85%, mainly due to the evaporation of crystalline water in the sample. The second inflection point is between 280 and 800 °C, and the corresponding weight loss is 1.91%, which is due to the oxidation of Co_3O_4 in air.[24] On the contrary, the TGA curve of

https://doi.org/10.1021/acsomega.3c09337
ACS Omega 2024, 9, 5002−5013

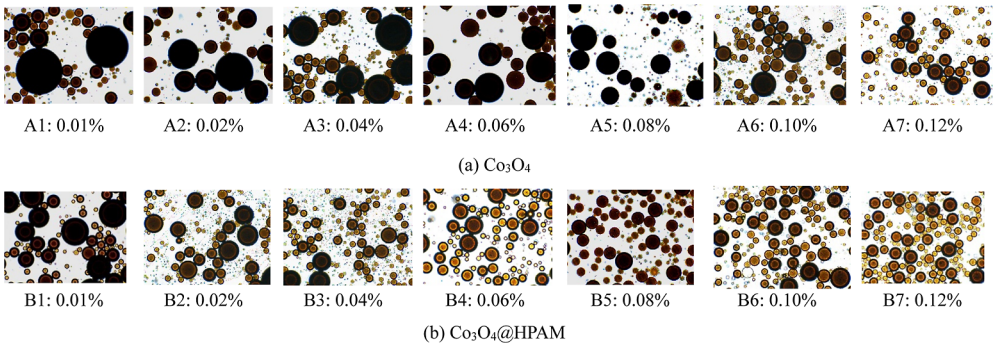

Figure 12. Oil droplet distribution under the effect of different mass fractions of MNPs before and after modification. (a) Co_3O_4 and (b) Co_3O_4@HPAM

Co_3O_4@HPAM shows three inflection points, which can be decomposed into three stages. Stage 1: at 35−230 °C, the weight loss is 15.67% due to the weight loss of residual water molecules and small molecule compounds remaining on the gel surface under heating; stage 2: at 250−480 °C, it is mainly caused by small molecules detached from cross-linking points or the decomposition of organic substances that appear to be broken, and the weight loss is 34.73%; and stage 3: at 480−800 °C, the weight loss is mainly caused by the imine reaction of amide group and thermal decomposition of the antelope, and the weight loss is 17.2%.[25,26] This phenomenon indirectly proves that Co_3O_4@HPAM has been synthesized successfully.

The microscopic morphology of Co_3O_4 and Co_3O_4@HPAM was observed by scanning electron microscopy (SEM), as shown in Figure 6.

The shape of the Co_3O_4 nanoparticles is essentially spherical, as shown in Figure 6a. In this study, HPAM was used to modify Co_3O_4 nanoparticles, as shown in Figure 6b, Co_3O_4@HPAM nanoparticles are embedded in the surface of a sponge-like gel, most of which are irregular spheres (Figure 6b). This phenomenon proves that Co_3O_4 @HPAM was successfully synthesized.

3.2. Effect of MNP Mass Fraction on the Stability and Rheological Property of Emulsion before and after Modification. *3.2.1. Effect of MNP Mass Fraction on Emulsion Stability before and after Modification.* Stability is an important evaluation index in the process of emulsification and viscosity reduction of heavy oil, and this section investigates the effect of the MNP mass fraction before and after modification on the water-separation rate of heavy oil-in-water O/W emulsion. In this experiment, the mass fraction of CAB-35 is 0.50%, the mass fraction range of MNPs before and after modification is 0.01−0.12%, and the emulsification temperature is 25 °C. The results are shown in Figure 7a,b.

From Figure 7a, it can be seen that under the effect of Co_3O_4, when the MNP mass fraction ≤0.02%, the water-separation rate of the emulsion is greater than that of the blank group; it can be learned that when the MNP mass fraction is low, it is not conducive to the stabilization of the emulsion. Then, with the increase of MNP mass fraction, the water-separation rate of the emulsion shows a downward trend. From Figure 7b, it can be seen that the water-separation rate decreases significantly in the presence of Co_3O_4@HPAM and shows a gradual decrease with the increase in mass fraction. When the mass fraction of Co_3O_4@HPAM is 0.04%, the water-separation rate can be reduced to 6.74%, which is 38.87% lower than that of the blank group, and the emulsion is more stable at this moment. With the continuous increase in its mass fraction, the decreasing trend of the water-separation rate is no longer obvious.

To make it easier to compare the effect of MNPs on emulsion stability before and after modification, the water-separation rate of 4 h is summarized in Figure 8.

As can be seen in Figure 8, when the mass fraction is 0.04%, the modified MNPs reduce the water-separation rate of the emulsion by 13 times more than the unmodified MNPs; At a mass fraction of 0.12%, the water-separation rate of the emulsion is 31.1% under the effect of unmodified MNPs. While under the effect of modified MNPs, the emulsion water-separation rate is only 1.69%. It is demonstrated that the modified MNPs can significantly improve the stability of the emulsion.

3.2.2. Effect of MNP Mass Fraction on Rheological Properties of Emulsion before and after Modification. Rheological property is another important evaluation index in the process of heavy oil emulsion viscosity reduction and transportation; therefore, this section investigates the effect of MNP mass fraction before and after modification on the rheology of heavy oil-in-water O/W emulsion. In this experiment, the mass fraction of CAB-35 is 0.50%, the range of MNP mass fraction range is 0.01−0.12%, and the emulsification temperature is 25 °C. The results are shown in Figure 9a,9b.

From Figure 9a, it can be seen that when the Co_3O_4 mass fraction was less than 0.02%, the apparent viscosity of the prepared emulsion decreased, but with the increase of the Co_3O_4 mass fraction, the apparent viscosity shows a gradual increase and the overall viscosity growth increases slightly.

From Figure 9b, it can be seen that the apparent viscosity of the heavy oil O/W emulsion increases gradually and more obviously with the increase of Co_3O_4@HPAM mass fraction. To illustrate the viscosity change more intuitively, the apparent viscosities at four different shear rates were therefore chosen and substituted into eq 2, and the viscosity reduction rate of the emulsion under the action of MNPs before and after modification with different mass fractions, as shown in Table 1.

As shown in Table 1, with the increase of the Co_3O_4 mass fraction, the emulsion viscosity reduction rate gradually decreases, but the viscosity reduction rate is more than 99%, and the overall variation range of the viscosity reduction rate is small. Combining with Figure 9 and Table 1, it can be found that the larger the apparent viscosity, the lower the viscosity reduction rate is. It can also be learned from the table that with the addition of Co_3O_4@HPAM, the viscosity reduction

https://doi.org/10.1021/acsomega.3c09337
ACS Omega 2024, 9, 5002−5013

Table 3. Comparison with the Results of Published Work

the results of other published work	the results of my research
Zhang et al.[14] prepared dual-responsive MNPs with Fe_3O_4 nanoparticles and $C_{12}min^+$ and found that the emulsion stability was enhanced in their presence because the combination of the two changed the three-phase contact angle of the nanoparticles and enhanced the hydrophobicity	we synthesized a polymer-based modified MNP by the aqueous solvation method and found that the use of this modified nanoparticle can significantly enhance the emulsion stability compared with the unmodified MNP
Gálvez-Vergara et al.[16] used polystyrene-modified MNPs to prepare switchable Pickering emulsions in mixtures of polar solvents (e.g., chloroform) and water. The surface of bMNPs was modified by free radical polymerization to give the nanoparticles enhanced hydrophobic properties	1. The reason is that the absolute value of the zeta potential of this Co_3O_4@HPAM-modified MNP is much larger than that of the Co_3O_4 MNP. The absolute value of the zeta potential of a Co_3O_4@HPAM-modified MNP is about 7 times that of a Co_3O_4 MNP when the mass fractions are both 0.04%, which greatly increases the electrostatic repulsion between oil droplets
Zhao et al.'s[37] use Polyethylenimine (PEI)-coated Fe_3O_4 MNPs were successfully synthesized for emulsion breaking by a one-step solvothermal method. The results showed that the emulsion-breaking efficiency increased with the increase in particle dosage. The presence of electrolytes facilitates oil removal, presumably by reducing the electrostatic repulsion or by altering the hydrophobicity of the MNP	2. Also, the contact angle of Co_3O_4 MNPs is only 30.98°, while the contact angle of Co_3O_4@HPAM-modified MNPs is 84.64°, which is closer to 90°. The modified MNPs have stronger hydrophobicity compared with Co_3O_4 MNPs, which is conducive to promoting the stability of O/W emulsions
Fan et al.'s[38] use of methyl- and octadecyl-grafted silica NPs, which have almost identical optimum contact angles, to stabilize emulsions dramatically reduced the effect of cooling on the viscosity	
Mendiratta et al.[39] report on the synthesis of novel "smart" based apatite (HAP) MNPs and their corresponding stimulus-responsive Pickering emulsions. Pickering emulsions prepared with our magnetic stearic acid-functionalized Fe_3O_3@HaP nanoparticles exhibit a pronounced pH-responsive behavior. We observed that the diameter of the emulsified droplets decreased with increasing pH	3. In addition, the modified MNPs further reduced the oil–water interfacial tension compared with MNPs. The combined effect of these mechanisms contributed to the stabilization of the emulsion

decreases with the increase of the Co_3O_4@HPAM mass fraction, but the viscosity reduction is more than 97%.

3.3. Effect Mechanism of MNP Mass Fraction before and after Modification on Emulsion Stability and Rheology. *3.3.1. Zeta Potentiometry.* It is considered that the positive and negative charge of MNPs will affect the chargeability of the oil droplets, which affects the stability of the emulsion.[27] To investigate the mechanism of the effect of the mass fraction of MNPs before and after modification on the stability of the emulsion, the zeta potential of the binary system of MNPs Co_3O_4 and Co_3O_4@HPAM compounded with CAB-35 and different mass fractions were tested. In the experiment, the mass fraction of CAB-35 is 0.50%, the mass fraction of MNPs before and after modification is in the range of 0.01−0.12%, and the testing temperature is 25 °C. The results are shown in Figure 10.

As shown in Figure 10, under the action of CAB-35 alone, the zeta potential measured in the solution is −5.5 mV; when the mass fraction of Co_3O_4 is less than 0.02%, the absolute value of the Zeta potential of the binary system composed of Co_3O_4 and CAB-35 is smaller than that of the blank group. When the mass fraction of Co_3O_4 continues to increase to 0.04%, the zeta potential is −6.51 mV, and then, with the increase of the absolute value of the mass fraction of MNPs, the absolute value of the zeta potential of the binary system increases gradually. When the mass fraction of Co_3O_4@HPAM is only 0.01%, the absolute value of the Zeta potential of the binary system composed with CAB-35 has been significantly increased to −29.6 mV, and then with the increase of the mass fraction of Co_3O_4@HPAM, the absolute value of the zeta potential of the binary system increases slowly, but the absolute value of the zeta potential of modified MNP is much higher than that of the unmodified.

From the above experimental results, it can be seen that when the mass fraction of unmodified Co_3O_4 is less than 0.02%, the absolute value of the zeta potential of the binary system is smaller than that of the blank group. At this time, the electrostatic repulsion between the oil droplets is smaller, which weakens the stability of the emulsion. With the increase of the mass fraction of MNPs, the absolute value of the zeta potential of the binary system gradually increases, which leads to the increase of the negative charge of oil droplets and the increase of the repulsive potential energy between oil droplets, making it more difficult for the oil droplets to aggregate with each other It shows that the water separation rate of the emulsion decreases at the macro level. Due to the negative charge of HPAM molecules on the surface of modified Co_3O_4, the absolute value of the Zeta potential of Co_3O_4@HPAM is significantly larger than that of unmodified Co_3O_4, resulting in a greater repulsion between oil droplets, more stable emulsion and lower water-separation rate, which is consistent with the significant enhancement of emulsion stability under the action of Co_3O_4@HPAM. The long chain of HPAM grafted with modified MNPs has a negative charge, and when it is dissolved in the aqueous phase, the hydrophilic branched chains stretch freely due to electrostatic repulsion. The higher the content of the polymer is, the more long-chain molecules dissolve in the bulk phase, resulting in an increase in the apparent viscosity of the emulsion.[28]

3.3.2. Contact Angle. Since the wettability of MNPs affects their adsorption properties on the oil−water interface,[27,29] this section studies the contact angle of MNPs before and after modification. The mass fraction of CAB-35 is 0.50%, and the

https://doi.org/10.1021/acsomega.3c09337
ACS Omega 2024, 9, 5002−5013

test temperature is 25 °C. The experimental results are shown in Figure 11.

As can be seen from Figure 11, the contact angle of Co_3O_4 before modification is only 30.98°, while that of Co_3O_4@HPAM after modification is 84.64°, which shows that the contact angle of the modified MNPs increases significantly, and the hydrophobicity is enhanced. Because the stronger the hydrophobicity of nanoparticles, the larger their free energy,[30] which makes it difficult for the nanoparticles adsorbed on the oil−water interface to desorb from the interface, providing a stronger spatial barrier for the droplets and thus preventing droplets from merging and improving the stability of emulsion. In addition, the long-chain molecules of HPAM branched on the surface of Co_3O_4 adsorbs on the surface of the oil droplets under the hydrophobic effect, which forms a heavy and viscoelastic adsorption layer on the one hand and increases the spatial site resistance on the other hand.[31] The combined effect of the above two causes the stability of the emulsion to be enhanced and the apparent viscosity of the emulsion to increase.

3.3.3. Interfacial Tension. The stronger the interfacial activity of the emulsifier, the more obvious the effect on the oil−water interfacial tension, and the addition of an emulsifier that can reduce the oil−water interfacial tension is a necessary condition for the formation of O/W emulsion.[32] Therefore, this section, by investigating the effect of Co_3O_4 and Co_3O_4@HPAM on oil−water interfacial tension, will further reveal the influence mechanism of the MNP mass fraction on emulsion stability before and after modification. The mass fraction of CAB-35 is 0.50%, the range values of the MNP mass fraction before and after modification are both 0.01−0.12%, the testing temperature is 25 °C, and the results of the oil−water interface test are shown in Table 2.

As shown in Table 2, under the action of CAB-35 alone, the oil−water interfacial tension is 1.56311 mN/m; when the mass fraction of unmodified MNPs Co_3O_4 is less than 0.02%, the oil−water interfacial tension is greater than that of the blank group, and then, with the increase in the mass fraction of the MNPs, the interfacial tension between oil and water decreases gradually. It can also be found that the oil−water interfacial tension is significantly reduced with the incorporation of modified MNPs Co_3O_4@HPAM. When the mass fraction is 0.04%, the oil−water interfacial tension is 1.48813 mN/m under the action of unmodified Co_3O_4, while under the action of Co_3O_4@HPAM, the oil−water interfacial tension reduces to 0.69382 mN/m. From this, it can be concluded that the incorporation of anionic-polymer-based modified MNPs can significantly reduce the oil−water interfacial tension, which is consistent with the variation of the water-separation rate.

3.3.4. Oil Droplet Distribution. The size and distribution of oil droplets have a close correlation with the overall stability of its emulsion. To further investigate the mechanism of the effect of MNPs on the aggregation of oil droplets before and after modification, the oil droplets of emulsion under the effect of different mass fractions of Co_3O_4, Co_3O_4@HPAM were observed using a microscope. The mass fraction of CAB-35 is 0.50%, the mass fraction of MNPs is all in the range of 0.01−0.12%, and the testing temperature is 25 °C. The distribution of oil droplets is shown in Figure 12.

Comparing Figure 12a,b, it can be found that with the increase of the mass fraction of MNPs, the large oil droplets gradually become smaller and more numerous; under the effect of modified MNPs, the large oil droplets gradually disperse into more small oil droplets as the mass fraction increases; when the mass fraction is only 0.04%, the oil droplets become small and uniform.

The reasons for the analysis are as follows: the smaller oil droplets have a larger surface area so that the emulsifier molecules in the emulsion can be more uniformly distributed at the oil−water interface, which effectively inhibits the fusion and aggregation of oil droplets because the adsorbent layer formed by the emulsifier can effectively isolate oil droplets and prevent them from contacting and aggregating; thus, it shows stronger stability. In general, emulsions with small droplet sizes are more resistant to gravitational separation and agglomeration than emulsions with larger droplets.[33] Smaller particle-size droplets increase the stability of the emulsion due to Stokes' law.[34] Combining Figures 9 and 12, the apparent viscosity of the emulsion gradually increases as oil droplets gradually become smaller and more, which is consistent with the study of Zhou et al.[35] The smaller the particle size of the emulsion, the higher the viscosity, the lower the flow index, and the emulsion shows strong shear-thinning properties. The yield stress and shear modulus of emulsions increase with a decrease in droplet radius.[36]

To facilitate an understanding of how this study differs from other published studies, the results with other published work are shown in Table 3.

4. CONCLUSIONS

Through the surface modification of Co_3O_4 MNPs and a series of physical characterization as well as regularity and mechanism experiments, it is proved that a polymer-modified MNP Co_3O_4@HPAM has been successfully synthesized, which can be effectively used for emulsification and viscosity reduction of heavy oils, and the conclusions are as follows:

(1) Compared with the unmodified MNPs, the modified MNPs have better dispersion and still maintain good dispersion at 120 min, which can enhance its effect.

(2) When the mass fraction of modified MNPs is 0.04%, the water separation rate of emulsion can be reduced to 6.98%, while when the mass fraction of unmodified MNPs is 0.12%, the water separation rate of emulsion is 31.1%. The apparent viscosity of the emulsion gradually increased with an increasing mass fraction of modified MNPs and increased from 0.104 Pa°s to 0.131 Pa°s at a shear rate of 300 s^{-1}. The use of modified MNPs can significantly improve the stability of the emulsion while the viscosity reduction rate is greater than 97%, which proves that the polymer-modified MNPs as emulsifiers of heavy oil-in-water emulsions not only significantly improve the stability of emulsions but also have the advantages of simple synthesis method, small dosage, etc., which can meet the needs of practical engineering applications.

(3) After the modification of Co_3O_4 with an anionic polymer, the contact angle of Co_3O_4 and the absolute value of zeta potential are greatly increased, and the interfacial tension is reduced. Before modification, the contact angle of Co_3O_4 is only 30.98°, and after modification, the contact angle of Co_3O_4 increases to 84.64°; when the mass fraction of modified Co_3O_4@HPAM is 0.01%, the absolute value of zeta point position of the modified Co_3O_4 @HPAM is −29.6 mV, which is much larger than that of the blank group (−5.5

https://doi.org/10.1021/acsomega.3c09337
ACS Omega 2024, 9, 5002−5013

mV) and the premodified Co_3O_4 (1.9 mV). Under the effect of the modified MNPs Co_3O_4@HPAM, the interfacial tension is two times lower than that of unmodified Co_3O_4; the oil droplets also showed smaller and more uniform distribution in the presence of polymer-modified MNPs Co_3O_4@HPAM. Under the above synergistic effect, the stability of the emulsion is significantly enhanced.

AUTHOR INFORMATION

Corresponding Author

Nana Sun − *College of Petroleum Engineering, Xi'an Shiyou University, Xi'an City, Shaanxi Province 710312, P. R. China*; Email: bingyuxuan6666@126.com

Authors

Jianbo Hu − *College of Petroleum Engineering, Xi'an Shiyou University, Xi'an City, Shaanxi Province 710312, P. R. China*; orcid.org/0000-0002-4173-9261

Yuli Ma − *College of Petroleum Engineering, Xi'an Shiyou University, Xi'an City, Shaanxi Province 710312, P. R. China*

Hongmei Dong − *College of Petroleum Engineering, Xi'an Shiyou University, Xi'an City, Shaanxi Province 710312, P. R. China*

Complete contact information is available at: https://pubs.acs.org/10.1021/acsomega.3c09337

Notes

The authors declare no competing financial interest.

ACKNOWLEDGMENTS

The authors wish to thank the Shaanxi Provincial Natural Science Foundation (2023-JC-YB-421), the Shaanxi Provincial Natural Science Foundation (2023-JC-QN-0467), the Xi'an Youth Science and Technology Lifting Project (095920221360) and the Xi'an Shiyou University Graduate Innovation and Practice Ability Training Program (YCS23213034) for financial support.

REFERENCES

(1) Martínez-Palou, R.; Mosqueira, M. d. L.; Zapata-Rendón, B.; Mar-Juárez, E.; Bernal-Huicochea, C.; de la Cruz Clavel-López, J.; Aburto, J. Transportation of heavy and extra-heavy crude oil by pipeline: A review. *J. Pet. Sci. Eng.* **2011**, *75* (3−4), 274−282.

(2) Fakher, S.; Ahdaya, M.; Elturki, M.; Imqam, A. Critical review of asphaltene properties and factors impacting its stability in crude oil. *J. Pet. Explor. Prod. Technol.* **2020**, *10*, 1183−1200.

(3) Dusan, D.; Vesna, K. M.; Veselin, B. Heating Cable Application in Solving Paraffin Deposition Problem in Tubing. *Pet. Sci. Technol.* **2010**, *28* (9), 969−978.

(4) Sugai, Y.; Komatsu, K.; Sasaki, K. et al. Microbial-induced oil viscosity reduction by selective degradation of long-chain alkanes. *Abu Dhabi International Petroleum Exhibition and Conference*; OnePetro, 2014.

(5) Mohammadi, S.; Sobati, M. A.; Sadeghi, M. Viscosity reduction of heavy crude oil by dilution methods: new correlations for the prediction of the kinematic viscosity of blends. *Iran. J. Oil Gas Sci. Technol.* **2019**, *8* (1), 60−77.

(6) Lv, S.; Peng, S.; Zhang, R.; Guo, Z.; Du, W.; Zhang, J.; Chen, G. Viscosity Reduction of Heavy Oil by Ultrasonic. *Petrol. Chem.* **2020**, *60*, 998−1002.

(7) Tang, X.; Chen, Y. B.; Guo, E. P.; et al. Experiment on Enhanced Oil Recovery by In-situ Catalytic Reforming of Super-heavy Oil. *Special Oil Gas Reservoirs* **2022**, *29* (1), 114−120.

(8) Li, X.; Zhang, F.; Liu, G. Review on new heavy oil viscosity reduction technologies. *IOP Conference Series: Earth and Environmental Science*; IOP Publishing, 2022; Vol. *983*; p 012059.

(9) Zhang, F.; Zhang, Q.; Zhou, Z.; Sun, L.; Zhou, Y. Study on the Effect of Different Viscosity Reducers on Viscosity Reduction and Emulsification with Daqing Crude Oil. *Molecules* **2023**, *28* (3), 1399.

(10) Liu, J.; Zhong, L.; Yuan, X.; Liu, Y.; Zou, J.; Wang, Q.; Zhang, W.; Zhang, H. Study on the re-emulsification process of water in heavy oil emulsion with addition of water-soluble viscosity reducer solution. *Energy Fuels* **2019**, *33* (11), 10852−10860.

(11) Józefczak, A.; Wlazło, R. Ultrasounds studies of emulsion stability in the presence of magnetic nanoparticles. *Adv. Condens. Matter Phys.* **2015**, *2015*, 398219.

(12) Shirokikh, S. A.; Klevtsova, E. O.; Savchenko, A. G.; Koroleva, M. Y. Stability of highly concentrated water-in-oil emulsions with magnetic nanoparticles and the structure of highly porous polymers formed on their basis. *Colloid J.* **2021**, *83* (6), 806−815.

(13) Yue, L.; Pu, W.; Zhao, T.; Zhuang, J.; Zhao, S. A high performance magnetically responsive Janus nano-emulsifier: Preparation, emulsification characteristics, interfacial rheology, and application in emulsion flooding. *J. Pet. Sci. Eng.* **2022**, *208*, 109478.

(14) Zhang, M.; Ma, X.; Yang, W.; Wang, F.; Yu, H.; Song, A. Dual-responsive Pickering emulsions triggered by CO2 and magnetism. *J. Mol. Liq.* **2021**, *341*, 116906.

(15) Luo, D.; Sun, N.; Li, Q. H.; et al. Preparation and modulation of Pickering emulsion stabilized by non-covalent hydrophobic modified nanoparticles. *CIESC J.* **2020**, *71* (4), 1859−1870.

(16) Gálvez-Vergara, A.; Fresco-Cala, B.; Cárdenas, S. Switchable Pickering emulsions stabilized by polystyrene-modified magnetic nanoparticles. *Colloids Surf., A* **2020**, *606*, 125462.

(17) Grein-Iankovski, A.; Loh, W. Modulating the interfacial properties of magnetic nanoparticles through surface modification with a binary polymer mixture towards stabilization of double emulsions. *Colloids Surf., A* **2020**, *586*, 124208.

(18) Uhlmann, P.; Merlitz, H.; Sommer, J. U.; Stamm, M. Polymer brushes for surface tuning. *Macromol. Rapid Commun.* **2009**, *30* (9−10), 732−740.

(19) Sun, N. N.; Shen, L. S.; Sun, H. N.; Hu, J. pH Responsiveness of Microwave Polymer-Type Modified Magnetic Nanoparticles for Synergistic Emulsion-Breaking Effect on Thick Oil. *SPE J.* **2023**, *28*, 2619−2628.

(20) Itteboina, R.; Sau, T. K. Sol-gel synthesis and characterizations of morphology-controlled Co3O4 particles. *Mater. Today: Proc.* **2019**, *9*, 458−467.

(21) Yu, C. Preparation of Hydrophobic Modified Polyacrylamide and Study on Selective Flocculation-Flotation. *Multipurp. Util. Miner. Resour.* **2021**, *1*, 199−203.

(22) Chen, G.; Li, L.; Zhu, Z.; Ouyang, J.; Wang, F.; Wang, Y.; Xue, J. Synthesis of Ultra High Molecular Weight HPAM and Viscosity Forecast by BP Neural Network. *Mater. Sci.* **2015**, *21* (4), 559−562.

(23) Gu, F.; Li, C.; Hu, Y.; Zhang, L. Synthesis and optical characterization of Co3O4 nanocrystals. *J. Cryst. Growth* **2007**, *304* (2), 369−373.

(24) Liu, L.; Zhou, Z.; Wang, C.; Xu, J.; Xia, H.; Chang, G.; Liu, X.; Xu, M. Superior thermochemical energy storage performance of the Co3O4/CoO redox couple with a cubic micro-nanostructure. *J. Energy Storage* **2021**, *43*, 103167.

(25) Li, J.; Yang, X.; Xie, T. J.; et al. Study on the properties of a temperature-resistant and salt-tolerant HPAM gel. *Appl. Chem. Ind.* **2022**, *51* (06), 1642−1646.

(26) Pu, W.; Du, D.; Liu, R.; Li, K.; Huang, T. Synthesis and evaluation of β-cyclodextrin-functionalized hydrophobically associating polyacrylamide. *RSC Adv.* **2016**, *6* (98), 96006−96014.

(27) Sun, N. N.; Hu, J. B.; Shen, L. S.; Sun, H.; Wang, D. Effect of modified γ-Fe2O3 magnetic nanoparticles on the stability of heavy oil-in-water emulsions. *J. Dispersion Sci. Technol.* **2023**, 1−10.

(28) Sun, N.; Jiang, H. Y.; Xie, Y. P.; et al. Effects of Amphoteric Surfactant/Polymer on Water Separation Rate and Viscosity-Reducing Rate of Heavy Oil-in-Water Emulsion. *Acta Pet. Sin.* **2018**, *34* (3), 600.
(29) Salari, J. W.; Leermakers, F. A.; Klumperman, B. Pickering Emulsions: Wetting and Colloidal Stability of Hairy Particles— A Self-Consistent Field Theory. *Langmuir* **2011**, *27* (11), 6574−6583.
(30) Ghouchi Eskandar, N.; Simovic, S.; Prestidge, C. A. Synergistic effect of silica nanoparticles and charged surfactants in the formation and stability of submicron oil-in-water emulsions. *Phys. Chem. Chem. Phys.* **2007**, *9* (48), 6426−6434.
(31) Li, M. Y.; Wu, Z. L. *Petroleum emulsion*; Science Press: Beijing, 2009; pp 173−174.
(32) Jiang, X.; Liu, M.; Li, X.; Wang, L.; Liang, S.; Guo, X. Effects of Surfactant and Hydrophobic Nanoparticles on the Crude Oil-Water Interfacial Tension. *Energies* **2021**, *14* (19), 6234.
(33) McClements, D. J. Enhanced delivery of lipophilic bioactives using emulsions: a review of major factors affecting vitamin, nutraceutical, and lipid bioaccessibility. *Food Funct.* **2018**, *9* (1), 22−41.
(34) Shi, X. y.; Gao, H.; Lazouskaya, V. I.; Kang, Q.; Jin, Y.; Wang, L. P. Viscous flow and colloid transport near air-water interface in a microchannel. *Comput. Math. Appl.* **2010**, *59* (7), 2290−2304.
(35) Zhou, L.; Zhang, W.; Wang, J.; Zhang, R.; Zhang, J. Comparison of oil-in-water emulsions prepared by ultrasound, high-pressure homogenization and high-speed homogenization. *Ultrason. Sonochem.* **2022**, *82*, 105885.
(36) Weiss, J.; McClements, D. J. Influence of Ostwald ripening on rheology of oil-in-water emulsions containing electrostatically stabilized droplets. *Langmuir* **2000**, *16* (5), 2145−2150.
(37) Zhao, H. T.; Zhang, C.; Qi, D.; Lü, T.; Zhang, D. One-step synthesis of polyethylenimine-coated magnetic nanoparticles and its demulsification performance in surfactant-stabilized oil-in-water emulsion. *J. Dispersion Sci. Technol.* **2019**, *40* (2), 231−238.
(38) Fan, Z.; Zhang, L.; Di, W. W.; Li, K.; Li, G.; Sun, D. Methyl-grafted silica nanoparticle stabilized water-in-oil Pickering emulsions with low-temperature stability. *J. Colloid Interface Sci.* **2021**, *588*, 501−509.
(39) Mendiratta, S.; Ali, A. A. A.; Hejazi, S. H.; Gates, I. Dual stimuli-responsive Pickering emulsions from novel magnetic hydroxyapatite nanoparticles and their characterization using a microfluidic platform. *Langmuir* **2021**, *37* (4), 1353−1364.

https://doi.org/10.1021/acsomega.3c09337
ACS Omega 2024, 9, 5002−5013